



HAL
open science

Contribution of multispectral (optical and radar) satellite images to the classification of agricultural surfaces

C. Marais Sicre, R. Fieuzal, F. Baup

► **To cite this version:**

C. Marais Sicre, R. Fieuzal, F. Baup. Contribution of multispectral (optical and radar) satellite images to the classification of agricultural surfaces. *International Journal of Applied Earth Observations and Geoinformation*, 2020, 84, 10.1016/j.jag.2019.101972 . insu-03668291

HAL Id: insu-03668291

<https://insu.hal.science/insu-03668291>

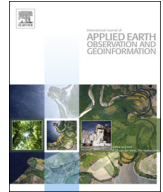
Submitted on 16 May 2022

HAL is a multi-disciplinary open access archive for the deposit and dissemination of scientific research documents, whether they are published or not. The documents may come from teaching and research institutions in France or abroad, or from public or private research centers.

L'archive ouverte pluridisciplinaire **HAL**, est destinée au dépôt et à la diffusion de documents scientifiques de niveau recherche, publiés ou non, émanant des établissements d'enseignement et de recherche français ou étrangers, des laboratoires publics ou privés.



Distributed under a Creative Commons Attribution - NoDerivatives 4.0 International License



Contribution of multispectral (optical and radar) satellite images to the classification of agricultural surfaces

C. Marais Sicre*, R. Fieuzal, F. Baup

CESBIO, Université de Toulouse, CNES/CNRS, IRD/UPS, Toulouse, France

ARTICLE INFO

Keywords:

Agriculture
Classification
Random Forest
Land use and land cover
Optical
Radar
Formosat-2
TerraSar-X
Radarsat-2
Alos PALSAR
Crops
Multi-frequency

ABSTRACT

The monitoring of different crops (cultivated plots) and types of surface (bare soils, etc.) is a crucial economic and environmental issue for the management of resources and human activity. In this context, the objective of this study is to evaluate the contribution of multispectral satellite imagery (optical and radar) to land use and land cover classification.

Object-oriented supervised classifications, based on a Random Forest algorithm, and majority zoning post-processing are used. This study emerges from the experiment on multi-sensor crop monitoring (MCM'10, Baup et al., 2012) conducted in 2010 on a mixed farming area in the southwest of France, near Toulouse. This experiment enabled the regular and quasi-synchronous collection of multi-sensor satellite data and in situ observations, which are used in this study. 211 plots with contrasting characteristics (different slopes, soil types, aspects, farming practices, shapes and surface areas) were monitored to represent the variability of the study area. They can be grouped into four classes of land cover: 39 grassland areas, 100 plots of wheat, 13 plots of barley, 20 plots of rapeseed, and 2 classes of bare soil: 23 plots of small roughness and 16 plots of medium roughness. Satellite radar images in the X-, C- and L-bands (HH polarization) were acquired between 14 and 18 April 2010. Optical images delivered by Formosat-2 and corresponding field data were acquired on 14 April 2010.

The results show that combining images acquired in the L-band (Alos) and the optical range (Formosat-2) improves the classification performance (overall accuracy = 0.85, kappa = 0.81) compared to the use of radar or optical data alone. The results obtained for the various types of land cover show performance levels and confusions related to the phenological stage of the species studied, with the geometry of the cover, the roughness states of the surfaces, etc. Performance is also related to the wavelength and penetration depth of the signal providing the images. Thus, the results show that the quality of the classification often increases with increasing wavelength of the images used.

1. Introduction

Knowledge of the land cover is an entry point for numerous applications calling upon the management of resources and human activity. The corresponding maps are thus a key element that can be used in many disciplines: to understand the territories, to monitor farming (Alcantara et al., 2013), for ecology (Qamer et al., 2016) or urban management (Lefebvre et al., 2016). A priori information is often necessary when such maps are drawn up and, to date, most regional and worldwide efforts to manage agro-ecological spaces have relied on sources of information collected from the field (statistics supplied by chambers and/or the ministry of agriculture) (McNairn et al., 2014; Pelletier et al., 2017).

However, the growing use of satellite imagery at very high spatial and temporal resolution enables land managers to obtain a variety of information on how land is used that is suitable for the scale at which they work, and remote sensing images form the foundations of ad hoc operational methods for monitoring agricultural surfaces from space. These images have been largely exploited in recent decades for mapping continental areas (Jacquemoud et al., 2009; Fig. 1; Waldner et al., 2015; Betbeder et al., 2015), studying crops (Bastiaanssen et al., 2000; Seelan et al., 2003; Hadria et al., 2009; Moran et al., 2012; Marais Sicre et al., 2016), identifying farming practices (Fieuzal et al., 2011; Marais Sicre et al., 2014, 2017), estimating biophysical parameters (Duchemin et al., 2006; Claverie et al., 2012; Atzberger, 2013; Duchemin et al., 2015; Baup et al., 2016; Betbeder et al., 2016), or estimating crop yields

* Corresponding author.

E-mail addresses: claire.marais-sicre@cesbio.cnes.fr (C. Marais Sicre), remy.fieuzal@cesbio.cnes.fr (R. Fieuzal), frederic.baup@cesbio.cnes.fr (F. Baup).

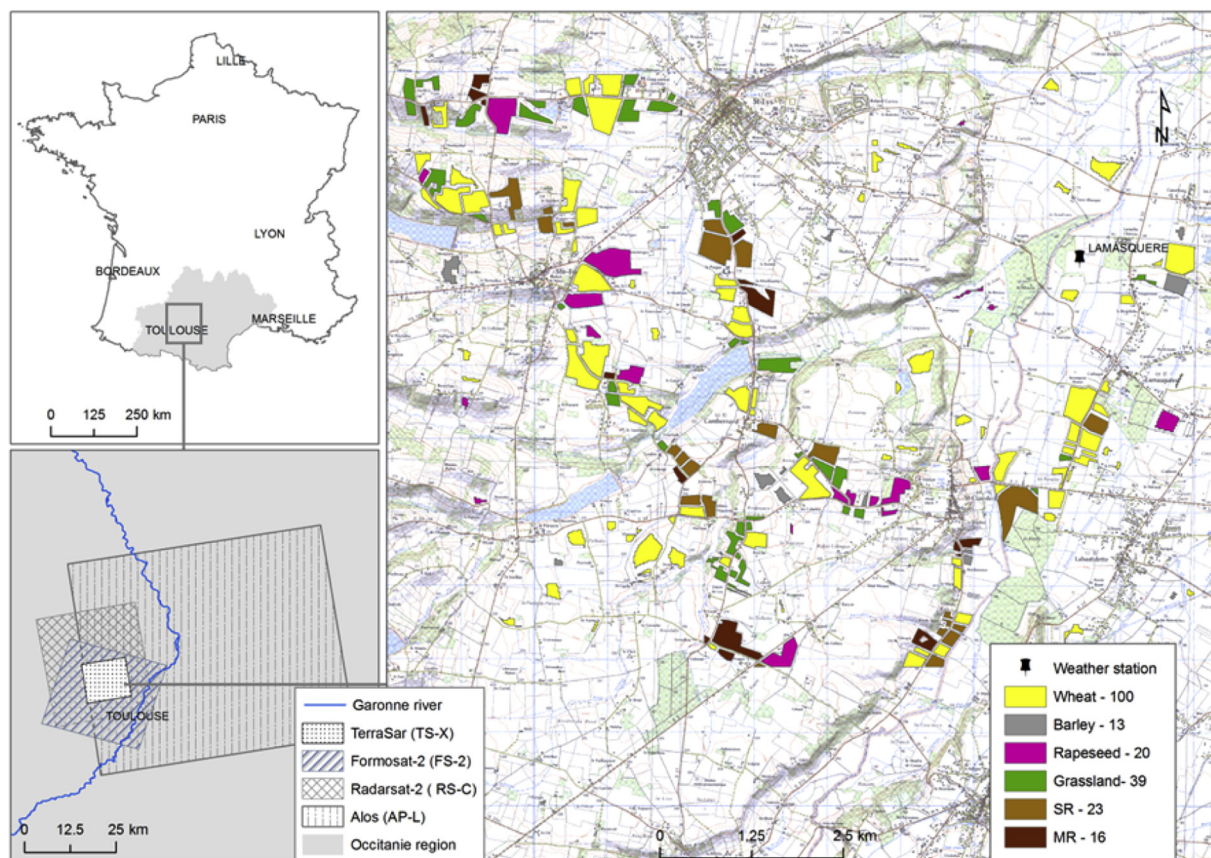


Fig. 1. Footprint covered by optical and radar imaging superimposed on the study site, and locations of the monitored plots (wheat, barley, rapeseed, grassland, small roughness (SR), medium roughness (MR) and quantity).

(Soria-Ruiz et al., 2009; Fieuzal and Baup, 2016; Fieuzal et al., 2017). These methods combine in situ data from observation networks with satellite images, principally acquired in the optical and, more recently, microwave ranges. Numerous studies have shown the ability of optical imagery to detect the type and state of a crop (Joshi et al., 2016) and the ability of radar images to follow surface states and stages of development (Hadria et al., 2009; McNairn et al., 2014). Given the complementary nature of optical and radar signals (notably their different penetration capacities), they have been used in synergy to improve the ways agricultural surfaces are monitored, including the accuracy of mapping and of biophysical parameter estimations (Amarsaikhan and Douglas, 2004; Blaes et al., 2005; McNairn et al., 2009a; Fiset et al., 2013; Hong et al., 2014; Inglada et al., 2016).

A variety of methods for detecting changes in land use by classifying multi-source, multi-temporal data have been proposed and evaluated in recent years (Lu and Weng, 2007; Mountrakis et al., 2011; Srivastava et al., 2012; Hussain et al., 2013; Tewkesbury et al., 2015). Their aim is to develop detection methods and/or to analyse the overall behaviour of the crops studied, and their results are acceptable. However, the possibilities offered by the use of complementary wavelengths to study the confusions affecting the different classes of land use are rarely considered, (Marais Sicre et al., 2017), and the performances of the satellite signals remain difficult to compare. On the one hand, the studies conducted at different sites present different, even specific, types of land use or surface states and, on the other, they rely on a limited number of satellite configurations (McNairn et al., 2009b).

Given the great difficulty of acquiring images at several wavelengths simultaneously, the present work focuses on a mono-temporal approach (acquisition dates centred on 14 April 2010) in contrast to other approaches, known as multi-temporal, in which the entire cultivation cycle can be followed. The mono-date approach gives globally

limited results (Dusseux et al., 2014; Schuster et al., 2015) but offers the surface state stability needed to estimate the contributions of the different satellite signals (surface roughness, humidity, land use, crop development, etc.). In this context, the objective of the present study is to determine the contribution that the different spectral domains, viz. the optical (blue, green, red and near infrared) and microwave (X-, C- and L-band) domains, can make to the classification of 6 types of land cover: wheat, barley, rapeseed and grassland; smooth surfaces, and surfaces of medium roughness. The classifications are made by the Random Forest (RF) and Support Vector Machine (SVM) algorithms on the basis of data collected during the MCM'10 experiments (Multi-spectral Crop Monitoring, (Baup et al., 2012)) conducted in 2010 at a site located in southwest France. It has been established that these two algorithms enable classifications to be made with both optical and radar images and generally give better results than the other supervised classifiers on agricultural surfaces (Breiman, 2001; Vapnik, 1979; Pal, 2005; Duro et al., 2012.; Loosvelt et al., 2012; Du et al., 2015; Pelletier et al., 2017).

The first section of the article presents the study site and the data used (satellite images and field data), the second section presents the method (data pre-processing, classification and post-processing algorithms), and the third section presents an analysis of the results. The potential of the different frequency bands and/or combinations of frequencies is considered through the general detection performance levels for different land occupations, and the performances for each type of land use are discussed.

2. Study site

The study site was located in southwest France, near the city of Toulouse (centred on coordinates 43°29'36"N, 1°14'14"E, Fig. 1). This

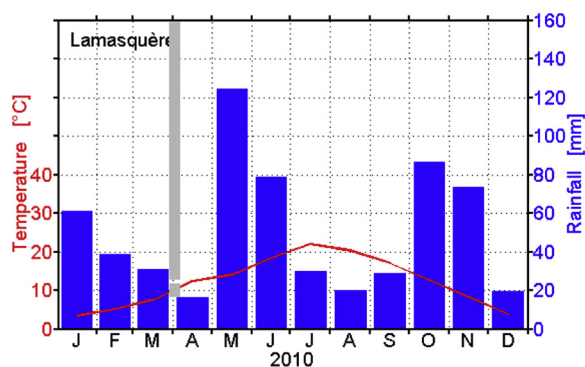


Fig. 2. Average monthly air temperature (in red) and the total monthly precipitation (in blue) collected by the weather station situated near the village of Lamasquère in 2010. The study period is indicated by the grey vertical line. (For interpretation of the references to colour in this figure legend, the reader is referred to the web version of this article.)

area is governed by a temperate climate, as shown by the data collected by the reference weather station situated near the village of Lamasquère. For 2010, the rainfall was measured at 600 mm, the extreme monthly values being recorded in April (18 mm) and May (125 mm). Large-amplitude temperature variations were also observed, with average air temperatures varying from a few degrees above freezing in winter to 25 °C in summer (Fig. 2). In this region of alluvial plains and hills, the steepest slopes (maximum 13.4°) are mainly found in the transition areas between low (174 m) and medium (319 m) altitudes (MCM'10, Baup et al., 2012; Marais Sicre et al., 2016).

The study site is mostly dedicated to farming activities (polyculture and livestock farming). It is mainly composed of agricultural plots (51.88%), allocated to winter or summer crops, and to permanent or temporary grasslands (22.27%). These serve as pasture, for the production of forage, or develop between two periods of cultivation. Finally, the landscape also comprises forests (18.06%), urban areas (built area, road...) (7.02%), and water reservoirs (0.76%).

3. Satellite images and field data

3.1. Optical and microwave satellite images

The study was based on images acquired in different wavelength ranges. Optical datas were provided from the Formosat-2 satellite, which delivers reflectance images in the blue, green, red and near infrared (respectively 0.45 to 0.52, 0.52 to 0.60, 0.63 to 0.69 and 0.76 to 0.90 μm), and microwave, with radar data from the TerraSar-X, Radarsat-2 and Alos satellites, which deliver signals in the X-band (λ = 3.1 cm), C-band (λ = 5.5 cm) and L-band (λ = 23.6 cm). The images were acquired within a 4-day interval (Table 1): on 14 April for TerraSar-X and Alos, 15 April for Radarsat-2, and 18 April for Formosat-2. Fig. 3 focuses on the different types of information relayed by optical and radar images.

TerraSar-X is a German Earth observation satellite that was launched in June 2007 and has a near-polar orbit. It provides radar images at high spatial resolution in several modes (Spotlight, Stripmap, and

ScanSAR), and with different polarization states (HH, HV, VV, and/or VH). The image of 14 April was acquired in Spotlight (SL) mode (2 m resolution on a 10 × 10 km² scene), on an ascending pass, with simple co-polarization (HH) and an incidence angle of 32.3°.

The Canadian Earth observation satellite Radarsat-2 was launched in December 2007 in a sun-synchronous polar orbit. It provides radar images in several modes, in simple co-polarization (HH, VV), and cross-polarization (HV, VH). The image of 15 April 2010 was acquired in Fine Quad Polar (FQP) mode, on an ascending pass, in the four polarization states. The resolution is close to 5 m, for a swath of 25 × 25 km², and an incidence angle of 30°.

Alos is a Japanese satellite launched in January 2006 in a sun-synchronous near-polar orbit. The image of 14 April 2010 was acquired in Fine Beam Single (FBS) mode on an ascending pass, in HH simple co-polarization. The image has a resolution of 6.25 m, a swath of 70 km, and an incidence angle of 38.7° (Jung et al., 2014).

Launched in May 2004 in a sun-synchronous orbit, the Taiwanese satellite Formosat-2 transports an array sensor providing high spatial resolution images with a constant viewing angle (lateral and front-to-back) of +/- 45° (Chern et al., 2006). The images have a spatial resolution of 8 m in multispectral (MS) mode. The image dated 18 April 2010, acquired in the framework of the "Kalideos" programme of the Centre National d'Etudes Spatiales (CNES), is centred on the study site and covers an area of 24 × 24 km².

The observations collected in situ concerned the identification of six categories of land use classes: three classes of field crops: wheat, barley and rapeseed, one class of grassland and two bare soilstates: Small Roughness, (SR) and Medium Roughness, (MR). To compensate for the time difference between the satellite passes and the gathering of in situ data, regular ground monitoring of the same plots enabled the land cover to be formally identified for a given date. Only the plots identified as having the same land use at the field observations of 14 and 30 April were kept.

The dataset was composed of 211 plots having contrasting characteristics (differences in slope, soil type, aspect, surface roughness, farming practices, shape and area) so as to reflect the variability of the study area (Fig. 1). This network of plots (with areas between 0.2 and 19.7 ha) enabled the spatial distribution and the heterogeneities observed in each of the classes considered to be described, together with the roughness associated with the surface states. Fig. 4 shows the phenological stages of the various crops and the types of bare soil present on the study site in April 2010. These surface states are placed in context in the time chart showing the development cycle of the field crops and grasslands (Fig. 5).

The "vegetated" plots are grouped into 4 land use classes: 39 plots of grassland (Fig. 4a–d), 100 of wheat, (Fig. 4e), 13 of barley (Fig. 4f), and 20 of rapeseed (Fig. 4g).

On 14 April 2010, the majority of grasslands were near peak greenness (Fig. 4a–d). However, they were composed of many plant species having their own growth cycles that rarely fully coincide. This great diversity could be seen in the fields as a broad range of heights (from 5 to 50 cm), colours (from yellow to green) and stages of development (growth phase, flowering, and senescence).

After a latency phase during the winter, the wheat, barley and rapeseed were in their spring growth phase (Fig. 5). On 14 April 2010, the

Table 1

Main characteristics of the optical and radar images (acquisition date, spectral band, polarization, mode, pass, incidence angle, resolution and swath).

	Acquisition date	Spectral band	Polarisation	Mode	Pass	Incidence angle (°)	Resolution (pixel size, m)	Swath (km)
TerraSAR (TS-X-HH)	14/04/2010	X	HH	SL	A	32,3	2	10
Radarsat-2 (RS-C-HH; RS-C-HV; RS-C-VV; RS-C-VH)	15/04/2010	C	HH-HV-VH-VV	FQP	A	30	5	25
Alos (AP-L-HH)	14/04/2010	L	HH	FBS	A	38,7	6.25	70
Formosat-2 (FS-2:B1-B2-B3-B4-MS)	18/04/2010	B-V-R-PIR	MS	MS	D	+/-45	8	24

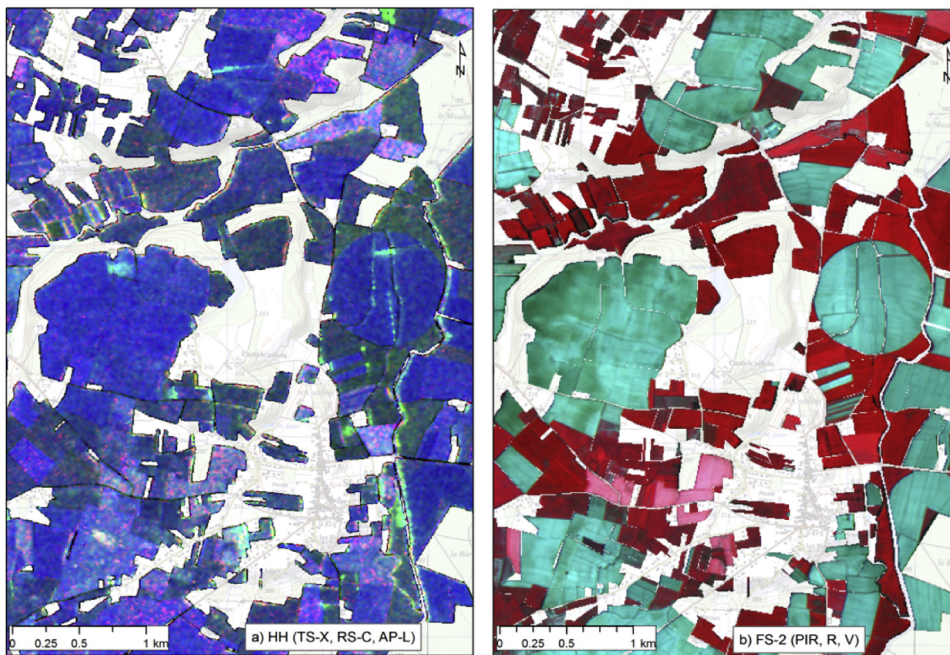


Fig. 3. Multi-frequency color-composed images based on a) radar data in HH polarization (TS-X, 04/14/2010; RS-C, 04/15/2010; AP-L, 04/14/2010) and b) an optical data (FS-2, 04/18/2010), superimposed on the transparent background of a "scan 25" map provided by the French National Geographic Institute (IGN). Reference field data.

barley was headed but this was not yet the case for the wheat, with a few exceptions linked to early sowing or the effects of different varieties (Fig. 4e and f). Wheat and barley had similar plant densities and an average height of 40 cm. Rapeseed was in flowering stage with an average height of 150 cm (Fig. 4g).

Finally, some plots had no vegetation. They had just been, or were about to be, sown with summer crops (hemp, maize, soybean, sorghum or sunflower) (Fig. 5). These plots were characterized by the level of roughness of their soil and two classes of surface state were distinguished. 23 plots had small roughness (SR) corresponding to a root mean square height, hrms, between 0 and 5 cm (Fig. 4h) and 16 plots had medium roughness (MR) corresponding to a root mean square height, hrms, between 5 and 10 cm (Fig. 4i). These differences in roughness level depended on the tools used to work the soil (discs, harrows).

3.2. Auxiliary data: Registre Parcellaire Graphique (RPG – graphic plot register)

The RPG is a geographic information system that obtains detailed information on land use and land holding structures, which is collected from farmers' declarations submitted to obtain subsidies from European administrative bodies. Since 2007, the services and payment agency makes a version of the RPG available in a regulated way, giving access to some of the data declared by the French farmers. The information is supplied for agricultural surfaces that cover one or more adjacent plots of different crops belonging to the same farmer (on average, 68% of these surfaces are made up of a single plot). The RPG for 2010 was used as a mask in the pre-processing phase of the present work, in order to restrict the study to cultivated areas only (crops and grasslands).

4. Method

The steps employed to analyse the contributions of the various satellite configurations and their complementarities for land use mapping are presented in Fig. 6. Various types of pre-processing were first applied to the satellite images according to their configurations. Segmentation based on the optical image was then performed to delimit the outlines of plots or homogeneous areas within a plot (Marais Sicre et al., 2014). The in situ observations, separated into two sets of

samples comprising 50% of the data, served for the object oriented supervised classification of the cultivated areas only (RPG mask). One set of samples was used for the learning phase and the other to validate the classification. This separation was carried out randomly, 10 times. Considering the stability of the results, with a kappa variance close to 3% (0.008 to 0.031), a sample taken in the average variance (variance 1.8%) was kept for presentation here. Majority zoning was finally applied to the classifications. The validation relied on different performance criteria established on the independent samples of the learning phase. These are analysed in the 'Results and discussion' section.

Finally, 25 classifications were carried out (Table 2), 11 mono-frequency configurations (optical reflectances, backscattering coefficients and polarizations separately) and 14 multi-frequency, multi-polarization or frequency combination cases (combinations of multi-spectral optical with a radar band, and multi-spectral optical and radar).

4.1. Image pre-processing

Various corrections: atmospheric, geometric and/or radiometric, were applied to the images according to the sensors considered. A geometric correction was applied to the optical images, with a final superposition accuracy of less than a half-pixel (Baillarin et al., 2008). These data were also processed for atmospheric effects in order to detect clouds and their shadows on the ground, and to correct perturbations in connection with aerosol effects (multi-temporal algorithm developed by Hagolle et al., 2008). Radiometric calibration of the TerraSar-X products was based on the procedure described by Fritz and Eineder (2008), using Eq. 1. The Radarsat-2 and Alos images were calibrated using the NEST software, which follows Eqs. 2 and 3 (MDA, 2000; Lavalle and Wright, 2009).

$$\sigma^i \text{ (dB)} = 20 \times \log_{10}(\text{DN}_i) + 10 \times \log_{10}(K) + 10 \times \log_{10}(\sin(\theta_i)) \quad (1)$$

$$\sigma^i \text{ (dB)} = 20 \times \log_{10}(\text{DN}_i/A2_i) + 10 \times \log_{10}(\sin(\theta_i)) \quad (2)$$

$$\sigma^i \text{ (dB)} = 20 \times \log_{10}(\text{DN}_i) + K \quad (3)$$

In the case of products delivered by TerraSar-X and Alos, the value of the backscattering coefficient (σ^0) at pixel i , depended on the digital number (DN), the calibration constant (K) and the incidence angle (θ). For Radarsat-2 products, a gain (A2) was also taken into account.

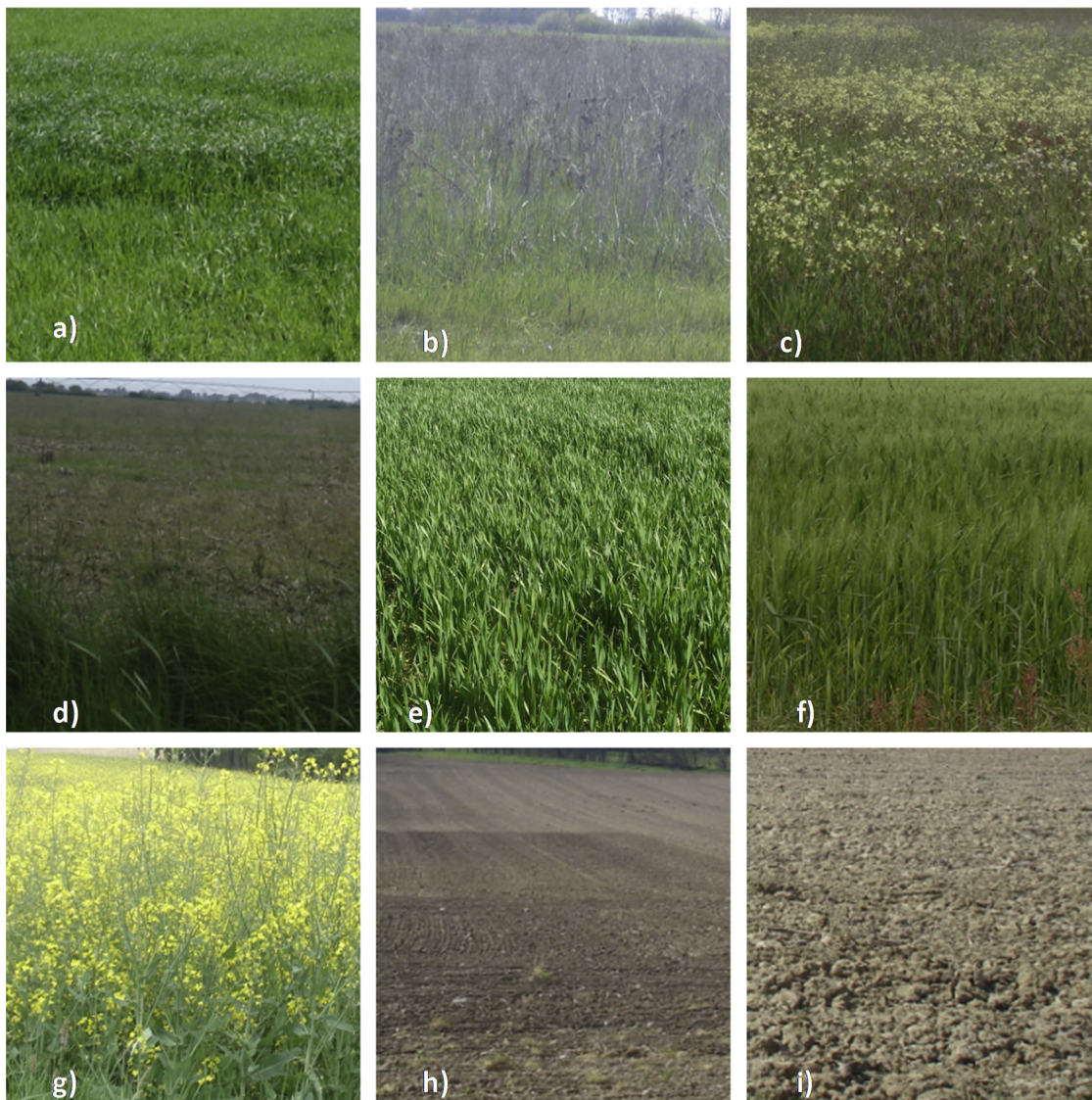


Fig. 4. Phenological stages of the different crops and surface states in April 2010: a), b), c) and d) 4 types of grassland; e) wheat, f) barley, g) rapeseed, bare soil with h) small roughness and i) medium roughness.

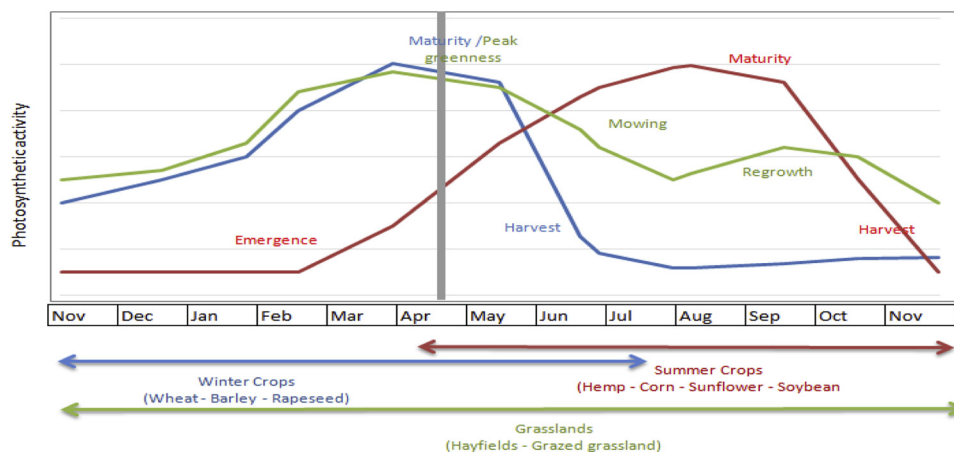


Fig. 5. Development cycles of winter crops, grasslands and summer crops. The grey vertical line represents the image acquisition period.

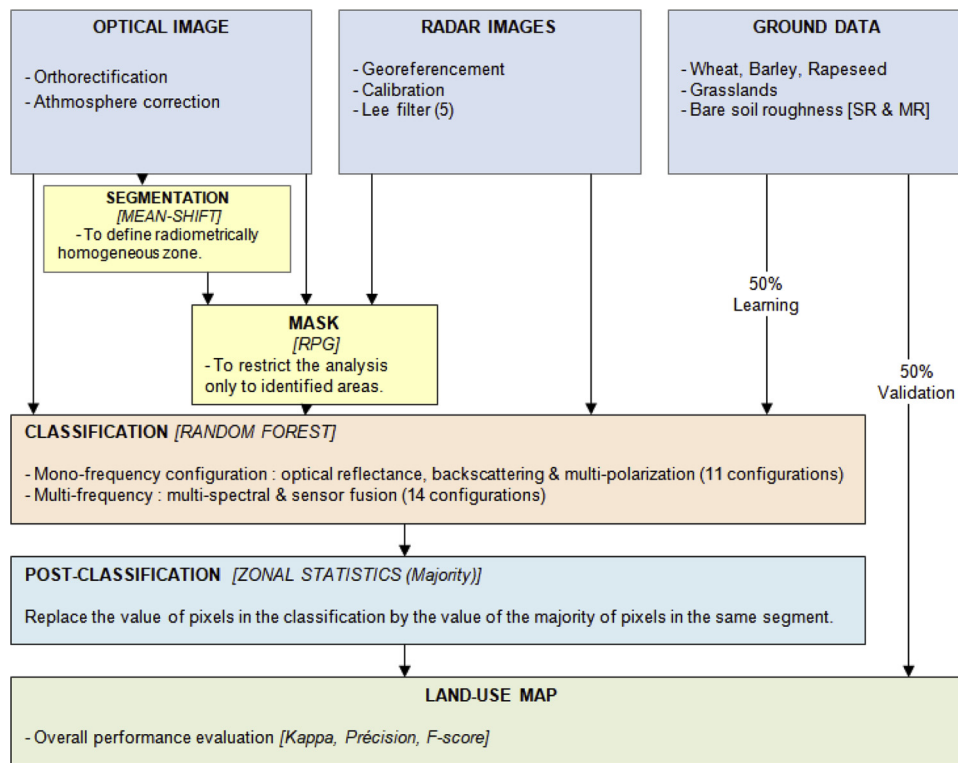


Fig. 6. Synoptic diagram of the steps employed for the land use mapping.

The radar images were geo-referenced on the basis of orthophotos supplied by the French National Geographic Institute (IGN). The resolution of the orthophotos (0.50 m) was degraded to correspond to the resolution of the different satellite products. Subsequently, the IGN image served as a reference to locate the 70 reference points for each of the SAR images. The geolocation accuracy was better than 10 m on average, considering the sizes of the pixels of the different products.

An improved Lee spatial filter (5 pixel window) was applied to the radar images to reduce speckle effects (Lee, 1981) and enhance the performance of the classifier. For classifications performed in mono-frequency, the native resolution of the images was kept (Table 1). For classifications generated by combining frequencies, the resolution of the least resolved image was used. Thus, the pixels of classifications made with Formosat-2 represented 8 m and those of the classification using all combinations of radar frequencies 6.25 m.

4.2. Segmentation

Segmentation aimed to delimit the borders of agricultural plots (units where land use is homogeneous) by means of the 'mean shift clustering' algorithm proposed by Comaniciu and Meer (2002), and implemented in the Orfeo Toolbox (open-source software, Michel and

Grizonnet, 2015). This algorithm identifies entities or segments by grouping together adjacent pixels that have similar spatial characteristics. It uses the four spectral bands of Formosat-2 images, which reproduce the outlines of simple land use units better than radar images can (limited by speckle effects).

The level of segmentation depends on the thresholds defined for three parameters: the spatial radius, the spectral radius and the minimum size of the area. For this study, the threshold values were set at 15, 15 and 100 pixels respectively. These parameters enable a defined quantity of pixels, having radiometric values that differ to a greater or lesser extent, to be brought together in a single segment so as to group related pixels by similarity of value. Thus, an agricultural plot can be defined by one or possibly several segments according to the heterogeneity within the plot. The segments resulting from such segmentation are radiometrically homogeneous and form an image where each pixel of a given segment is identified by a single label (4006 segments were generated in this study). The similarity of reflectance of the various land uses in the optical range at this moment of the phenological cycle constitutes a limit for obtaining the outline of a land unit corresponding to a given land use at a given date; contiguous plots with different land uses can be grouped together in a single segment and a heterogeneous plot can correspond to several segments.

Table 2
Recapitulation of configurations used for the classifications.

Mono-spectral/Multi-polarisation		Multi-spectral/Multi-polarisation	
Optic	Radar		
FS-2-B1	TS-X-HH	FS-2-MS	RS-C (HH) + FS-2-MS
FS-2-B2	RS-C-HH	RS-C-HH/HV	RS-C (HV) + FS-2-MS
FS-2-B3	RS-C-HV	RS-C-VV/ VH	RS-C (VV) + FS-2-MS
FS-2-B4	RS-C-VV	TS-X + RS-C + AP-L	RS-C (VH) + FS-2-MS
	RS-C-VH	TS-X-HH + RS-C-HH + AP-L-HH + FS-2-MS	RS-C (HH/HV) + FS-2-MS
	RS-C-FP	TS-X (HH) + FS-2-MS	RS-C (VV/ VH) + FS-2-MS
	AP-L HH	AP-L-HH + FS-2-MS	RS-C (HH/HV/VV/ VH) + FS-2-MS

4.3. Classifications

The classifications were tested by using the Support Vector Machine (SVM) and Random Forest (RF) classifiers implemented in the Orfeo ToolBox (version 5.0). The SVM classification, developed in the 1980s (Vapnik, 1979; Cortes and Vapnik, 1995; Burges, 1998) is non-parametric. Two classes are separated by a hyperplane that is defined as optimal if it maximizes the distance separating it from the examples it is closest to. The review written by Mountrakis et al. in 2011 shows that this algorithm, which is pertinent for crop detection, is used in the same way whatever the considered type of images (optical or radar). The RF classification developed by L. Breiman and A. Cutler in 2001 is also a multi-source, supervised, non-parametric classifier, which shows great promise as far as agricultural spaces are concerned (Gislason et al., 2006; Loosvelt et al., 2012). RFs are sets of classifiers that combine an aggregation technique known as "bagging", and a special technique for inducing decision trees (Loosvelt et al., 2012). Seeing the similarity between the results obtained with these two classifiers (mean difference in mono-frequency classifications less than 1%), only the results obtained with RF (algorithm taking much less computation time) are presented below.

4.4. Post-processing

A majority zoning algorithm was applied to the classifications (average improvement 3%). In each segment, the majority land use class was assigned to all pixels (Fig. 7).

4.5. Classification performance assessments

Validation was performed, based on the number of pixels, by means of a confusion matrix (Congalton, 1991). The performance indices used for overall pertinence were the kappa (relative difference between the proportion of agreement observed and the proportion of random agreement) and the OA (overall accuracy, ratio of correctly classified elements to total number of elements examined) (Eq. 4).

For the accuracy of each class, the classifications were evaluated

from the rates of True Positives (Tp), False Positives (Fp) and False Negatives (Fn) (Congalton, 1991), which were combined to calculate the Precision (P), the Recall (R) and the F-score.

The false positive rate quantified the pixels coming from the reference data that were wrongly placed in other classes. The false negative rate quantified the pixels that were placed in one class but actually belonged to another.

$$OA = \frac{Tp + Tn}{Tp + Tn + Fp + Fn} \tag{4}$$

The precision and the recall (Eq.s (6),(7)) corresponded, respectively, to the percentage of pixels coming from the reference class that were assigned to the right group, and to the percentage of correctly classified pixels with respect to the total number of pixels in the class. These parameters enabled the F-score to be deduced (Eq. (5)), which corresponded to the harmonic average of the precision and recall (Van Rijsbergen, 1979; Powers, 2011). This score has the advantage of falling strongly when one of the parameters (P or R) is low, and of increasing when the two parameters are close and high. The confusions affecting the different land use classes correspond to the harmonic mean of false negatives and false positives.

$$F - score = \frac{2 \times P \times R}{P + R} \tag{5}$$

with

$$P = \frac{Tp}{Tp + Fp} \tag{6}$$

$$R = \frac{Tp}{Tp + Fn} \tag{7}$$

5. Results and discussion

5.1. Overall performances

The overall performances (kappa) of the classifications varied between 0.35 and 0.81, with an overall accuracy ranging from 0.47 to

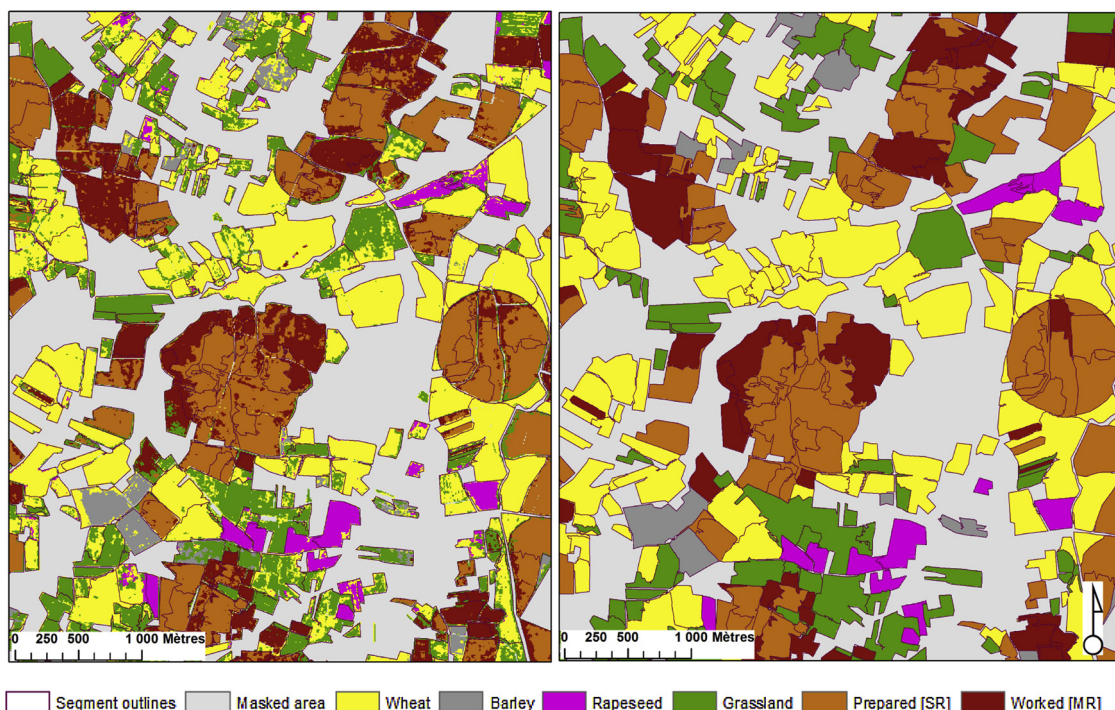


Fig. 7. Classification of the agricultural areas based on Alos and Formosat-2 images, before a) and after b) application of a majority zoning algorithm.

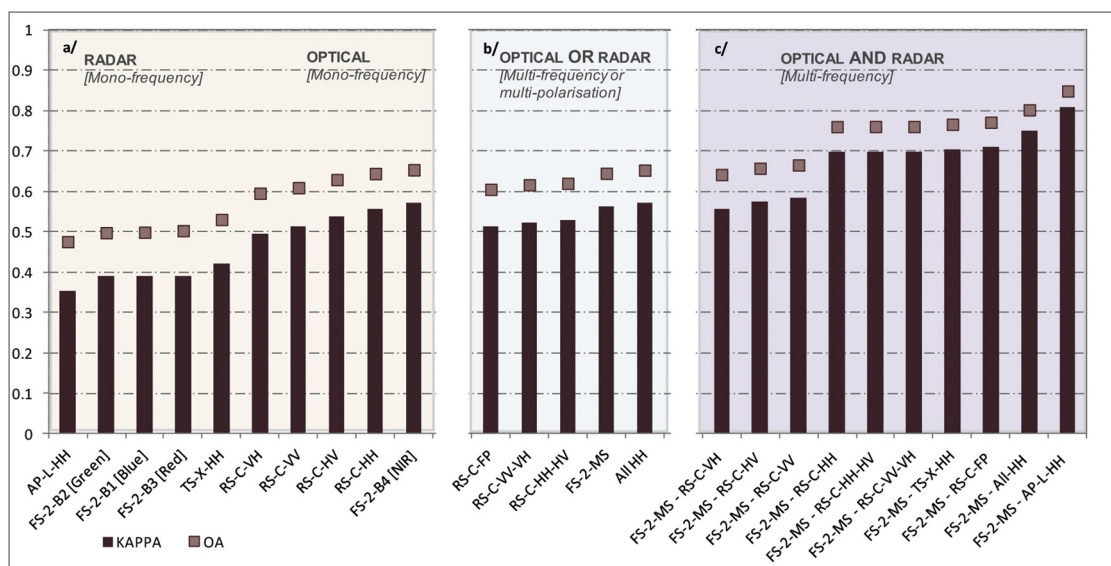


Fig. 8. Overall performances of classifications: kappa (histograms) and OA (squares) for each tested satellite configuration: radar or optical configurations alone in pink (a), multi-frequency optical or radar multi-polarizations in blue (b), or optical and radar fusion in mauve (c). (For interpretation of the references to colour in this figure legend, the reader is referred to the web version of this article.)

0.85 (Fig. 8). The best mono-frequency results were fairly poor and were obtained from the image acquired in the near infrared, with a kappa of 0.57 (FS-2-B4), whereas the highest value found for the other optical reflectances was 0.39. In the optical range, these poor performances should be considered with respect to the photosynthetic activity of the monitored ground cover classes (Fig. 4) at this moment of their phenological cycles. In April, the "vegetated" classes: winter crops and grassland, are visually very similar, in terms of both ground cover and development stage (Fig. 5) and have very similar reflectances. The different roughness states of bare soil also have very close reflectances (Corgne et al., 2014; Fieuzal et al., 2012). In the microwave domain, the results show marked contrast, with a minimum kappa of 0.35 for the L-band, 0.42 for the X-band and a maximum of 0.56 for the C-band (where the values vary between 0.52 and 0.56, depending on the considered polarization). Regarding the radar images, the classifier performances, in the case of "vegetated" classes (crops, grasslands), should be considered with respect to biophysical parameters that affect the intensity of the backscattered signal. The soil moisture content, the orientation of the rows of crops, the height of the plants, non-uniform development of the vegetation, the roughness, etc. affect the intensity of the radar signal for each pixel, independently of the considered class. In addition, the contribution of the vegetation to the backscattered signal evolves as the vegetation develops. Leaves, stalks and or fruits result in volume diffusion, single or double reflections that vary with the architecture of the crop (Picard et al., 2003; Betbeder et al., 2016; Fieuzal and Baup, 2016). Taking these parameters into account during the classification can thus increase the confusions among classes of crops having very different reflectances or, conversely, help to separate classes of crops that have similar reflectances on a given date (Ulaby et al., 1987; Steele-Dunne et al., 2017).

The multi-polarization approach in radar or MS in optical does not improve the performances (Fig. 8b). The NIR band contains all the relevant information of the optical range since using multi-spectral data reduces the kappa very slightly (-0.01).

Joshi et al. (2016), or Inglada et al. in 2016, demonstrated the advantage of the combined use of optical and radar signals, whatever the radar frequency, for all crops and chosen periods. Similar results were observed in the present study, where the combined use of optical and radar images (Fig. 8c) allowed crops to be better discriminated. In the majority of cases, the classification results improved significantly, with Kappa values between 0.55 and 0.81 (OA FS-2-MS/RS-C-VH = 0.64

and OA FS-2-MS/AP-L-HH = 0.85). The gain in performance was moderate for the combinations FS-2 MS with RDS-2 HV or RDS-2 VH, with a kappa remaining below 0.60. The other combinations gave a better kappa, between 0.70 and 0.81. This result emphasizes the complementarity of very different wavelengths, as illustrated by the combination of FS-2 MS and AP-L, which gives a Kappa greater than 0.81 in mono-date (OA = 0.85). The increase in Kappa relative to the classification using AP-L-HH alone is 57% and 31% for FS-2 MS. The optical/radar combination thus takes advantage of the different sensors and breaks free of the limits inherent in mono-date.

5.2. Performances by land use

Figs. 9–11 present the F-score (triangles) and the precision P (lozenges) (Eqs. (5), (6)) for each categories of land use classes. Histograms define confusions, with specific colours for each considered classes. Their analysis points out frequency complementarities. The land use classes are grouped together in three categories that correspond to the farming reality: winter crops (wheat, barley and rapeseed), grasslands, and the roughness states of bare soil.

5.2.1. Winter crops

Fig. 9a shows the classification results for wheat, Fig. 9b presents the same thing for barley and Fig. 9c for rapeseed. Globally, for these three land use classes, the performances of the classifications (F-score) are between 0.15 and 0.98 ($0.20 < P < 1$, Fig. 9). The best classifications have an F-score of 0.98 for rapeseed (for 4 configurations: AP-L-HH/FS-MS; RS-C-FP/FS-MS; TS-X-HH/FS-MS and All-HH/FS-MS), and 0.80 for wheat (FS-2-B4) with a precision always lower than the F-score (i.e., the false positive rate is higher than the false negative rate). The wheat class is thus overestimated in all the classifications, at the expense of barley. Such result is explained by the similarities in terms of phenology and architecture of these classes, and consequently very close levels of reflectance on satellite images. For example, the percentage of reflectance in the NIR for the wheat class is 39.6 and 39.8 for the barley class. In addition, part of the overestimation of the wheat class can be explained by the fact that wheat was strongly represented in the sampling (41% of the surface area sampled), which induced a bias in the learning phase (Chen et al., 2004; Mellor et al., 2015). For the barley class, the F-score never reached 0.60 (Fig. 9b).

In the optical range, the plots of wheat are well identified, with an

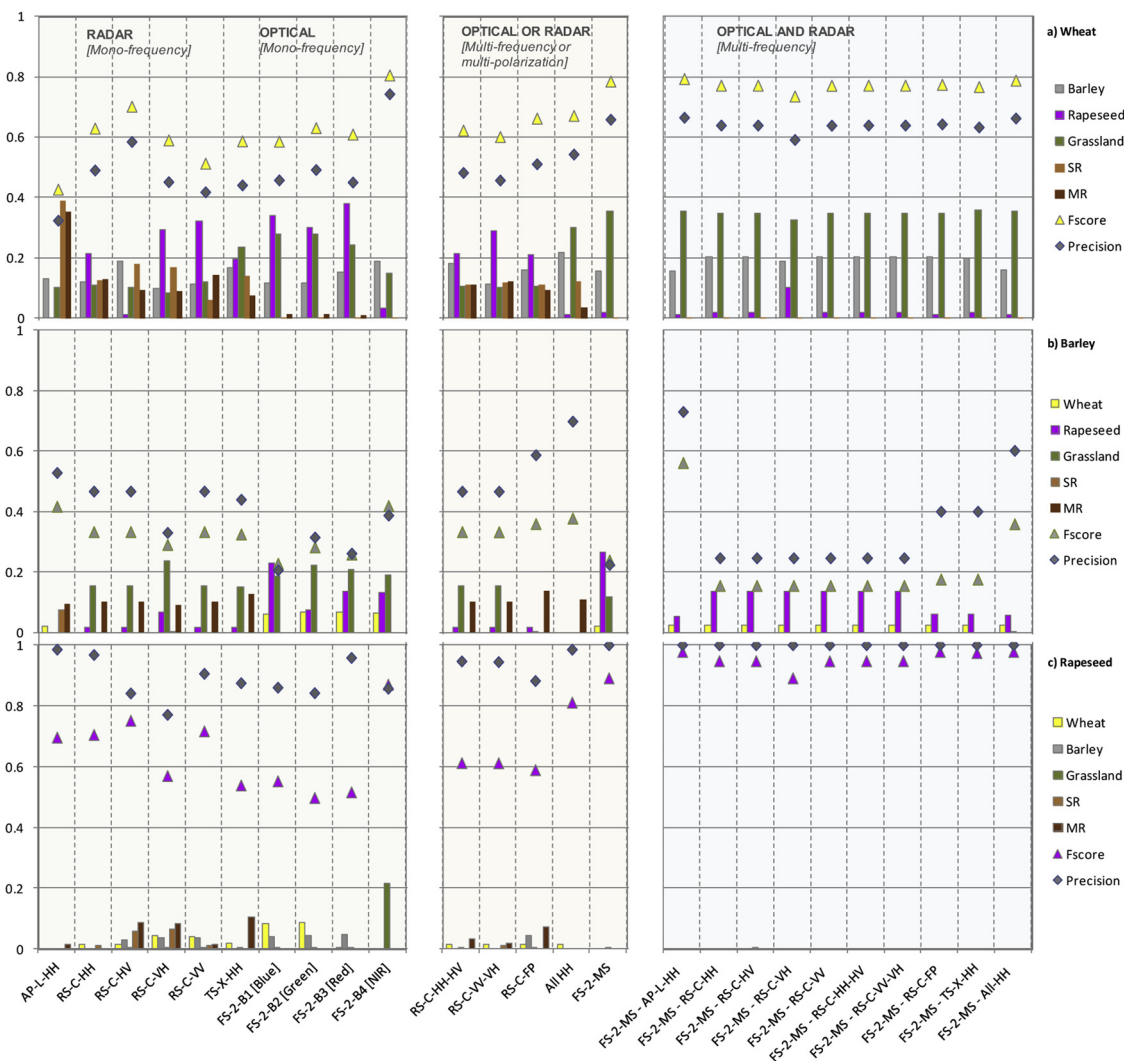


Fig. 9. Classification performance for each winter crop: F-Score (triangles) and class accuracy (lozenges), precision with the associated confusions (histograms) for: a) wheat (yellow), b) barley (grey), c) rapeseed (pink), for each tested satellite configuration. (For interpretation of the references to colour in this figure legend, the reader is referred to the web version of this article.)

F-score between 0.58 and a maximum of 0.80 for the near infrared band. However, this wavelength domain leads to confusions with rapeseed, grassland and barley, which differs according to the considered wavelength (Fig. 9a). This phenomenon can mainly be explained by the sensitivity of optical data to photosynthetic activity during this period

of vegetation growth, and the morphological similarity between cereals and grass at this moment in the phenological cycle (Fig. 4). In radar imaging, the results show an F-score between 0.42 for the L-band and 0.70 for the C-band in HV polarization. Confusions between plots of wheat and bare soil appear in the radar images. This can be explained

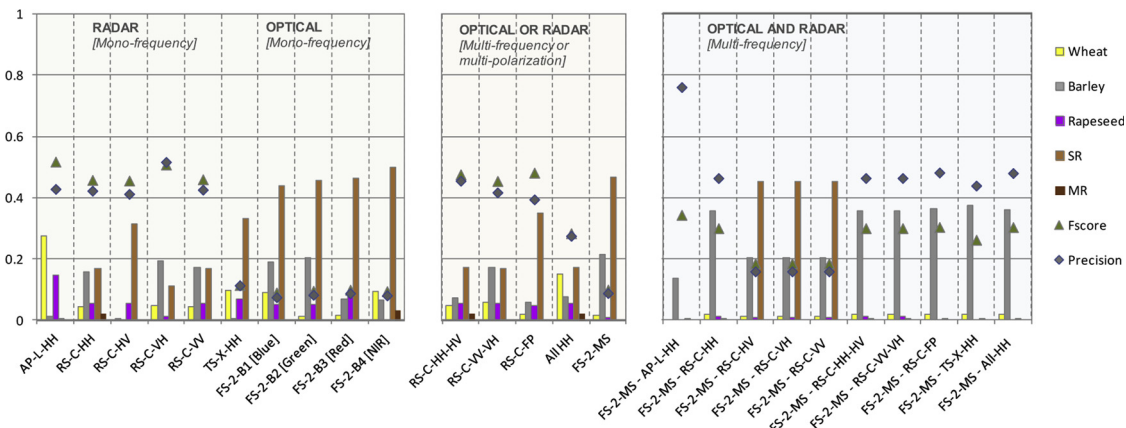


Fig. 10. Classification performance for grasslands: F-Score (triangles) and precision (lozenges) and associated confusions (histograms).

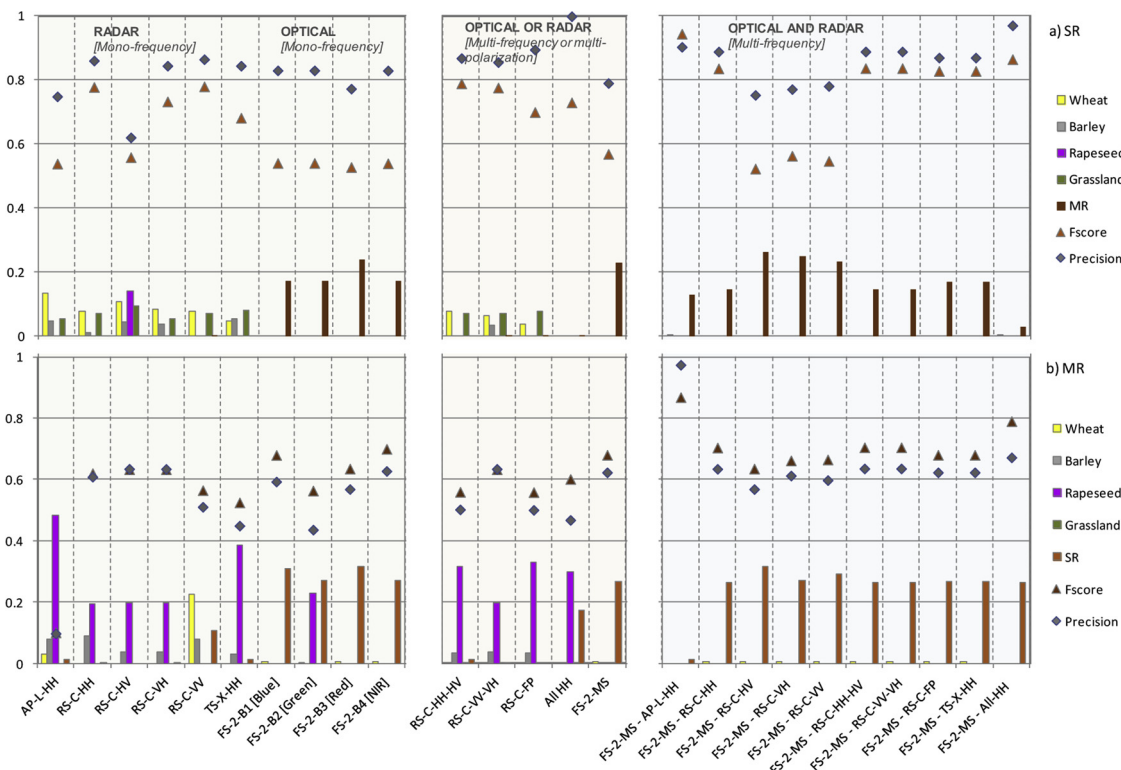


Fig. 11. Classification performance for bare soil classes: F-Score (triangles) and precision (lozenges) with the associated confusions (histograms) for: a) small roughness, SR (orange), b) medium roughness, MR (brown), for each satellite configuration tested.

by a contribution of the soil to the backscattering value, which increases with the depth of penetration of the wave (Picard, 2002; Fieuzal et al., 2013). The roughness of the soil in the plots of wheat can be greater or smaller depending on how the soil was worked before sowing. With a crop height ranging from 30 to 50 cm at this period of the cycle, the soil contribution has a different impact on the signal according to the considered radar wavelength. The high rates of confusion with the bare soil classes in the L-band illustrates such phenomenon (the cumulated F-score of the confusions with the bare soil classes, SR & MR, is 0.74) and, to a lesser extent, those observed in the C-and X-bands (cumulated F-score of the confusions with bare earth: 0.25 in C-band and 0.15 in X-band).

The radar or optical/radar multi-frequency combinations do not improve the performances obtained in optical multi-frequency. The confusions with bare soil are absent and only confusions with surfaces under grass or barley remain. Combination helps only with confusions specific to radar. Nevertheless the results remain less pertinent than when the infrared band is used alone, so it is of no interest to mutualize spectral or polarimetric information for wheat at this period of the phenological cycle.

The results obtained for barley are mediocre in both the optical and radar domains, with F-scores lower than 0.5 (Fig. 9b). In the optical range, the information is contained in the near infrared and the confusions are explained by the similarities of phenological stage of the winter crops and the grasslands (§3.2), for which the reflectances are very close. For radar, the confusions affect the grasslands and bare soil with medium roughness (MR) for the same reasons as those mentioned for wheat (i.e., the soil contribution). For example, the percentage of average reflectance for Alos for the barley class is 3.5 and 3.4 for the MR class. The radar multi-frequency combinations bring little improvement to the performances but the Full polar and All HH combinations avoid confusions of crops and grass, which shows the impact the geometry of the cover has in this period when ears are emerging (Fieuzal et al., 2013).

In a large majority of cases (80%), fusing optical and radar data degrades the classification performances with respect to the initial classifications ($P < 0.2$ and $F\text{-score} \leq 0.4$). Nevertheless, it is very important to note that fusing L-band image and data from Formosat-2 (MS) supplies some key information for the classification. This combination reveals the complementary nature of L-band (F-score AP-L-HH = 0.41) and Formosat-2 MS (F-score FS-2-MS = 0.23) wavelengths and enables an F-score of 0.56 to be obtained, together with a precision of 0.73. This can be explained by the fact that the confusions affecting the classification based on Alos (with bare soil and to a lesser extent with wheat) and those affecting the classification based on the reflectances of Formosat-2 image (with vegetated areas) largely offset each other. This complementarity is not found for the other combinations of optical and radar data. Thus confusions of barley with bare soil (peculiar to radar) and with grassland (present in optical and radar), completely disappear when the sensors are used in combination.

Rapeseed is well distinguished whatever the wavelength ($0.50 < F\text{-score} < 0.98$). For the optical range, the F-score with Formosat-2 MS reaches 0.89. Regarding confusions, there is true complementarity among the different wavelengths at this moment of the rapeseed phenological cycle (in flower) since confusions observed in the mono-frequency classifications disappear completely when the multispectral domain is used. For radar, the F-score RS-C-HV reaches 0.75. As for optical data, the confusions with bare soil that exist on radar mono-frequency classifications totally disappear when using all the frequencies in HH polarization.

These performance levels improve further when optical and radar frequencies are used in combination, reaching 0.98 in four different combinations (AP-L-HH/FS-MS, TS-X/FS-MS, All-HH/FS-MS and RS-C-FP/FS-MS).

5.2.2. Grasslands

The F-score values associated with grasslands are between 0.09 and 0.52 ($0.08 < P < 0.76$) (Fig. 10). The classifications based on signals

Table 3
Accuracy evaluation.

	Positive classification	Negative classification
Positive reference	TP	FP
Negative reference	FN	TN

acquired at short wavelengths which are characterized by small penetration depths (X-band, blue, green, red and NIR) show mediocre performance levels and high confusion with bare soil of small roughness. These confusions can be explained by the closeness of the mean reflectance levels and by the high dispersion of the satellite signals observed on these surfaces which are highly heterogeneous (Fig. 4). Conversely, the use of images acquired at longer wavelengths (L-band and C-bands for all polarizations) improves the classifications, with F-score between 0.46 and 0.52, even though confusions with smooth bare soil persist when the C-band is used. The best results are obtained in the L-band, with an F-score reaching 0.52 and some confusions with wheat and rapeseed classes. The Alos image allows soil roughness to be discriminated and thus avoids confusion with bare soil. The sensitivity of the satellite signal to the architecture of the vegetation allows confusion between grasslands and barley to be completely avoided when the barley ears emerge.

The use of polarization combinations in the C-band does not improve the results obtained in simple co-polarization, and the combination of all the frequencies with HH polarization degrades them. Similar result is observed for the combination of MS optical images and radar images, which gives F-scores lower than those obtained with the Alos, Radarsat-2, or optical images used alone. The combination of MS images with C-band is not a relevant choice, as evidenced by the degraded F-score values, compared with the results for C-band alone. In this case, adding optical data induces more noise than signal useful to the classification.

From a user point of view, the best results are obtained by combining the MS images and those acquired in the L-band (PFS-2-MS-AP-L = 0.76) (Marais Sicre et al., 2017). They avoid most of the confusions observable on classification based on multi-spectral or C-band image. These results are in accordance with the study presented by (Schuster et al., 2015), showing the limitations of optical images (visible and NIR) and X-band radar for mapping grasslands at a given date (Schuster et al., 2015). Moreover, the present study extends the results to other frequencies, highlighting the interest of combining MS and L-band images. In such case, the radar signal provides a complementary information, L-band data being sensitive to biomass (Hill et al., 2005).

5.2.3. Bare soil roughness levels

Fig. 11 a presents the performances of classifications obtained for bare soil with small roughness (SR) together with the confusions affecting this land use class, and Fig. 11b presents the results concerning bare soil with medium roughness (MR). The F-scores associated with these two levels of bare soil roughness are between 0.10 and 0.94 ($0.10 < P < 0.99$). The almost similar bare soil reflectance values observed whatever the optical wavelength explains the confusion between the two classes of roughness. For example, the percentage of average reflectance in the blue is 8.2 and 7.1 for classes MR and SR, respectively. In contrast, there are few confusions with the crop classes where the average reflectance in the blue is less than 4%. The opposite occurs in the microwave domain, where the confusions are mainly observed with crops classes and marginal between the soil roughness states. Indeed, the backscattered signal is weaker for smooth soil than for rougher and vice versa (Fieuzal and Baup, 2016; Baghdadi et al., 2002, 2016).

For bare soil of small roughness, the classifications based on optical reflectances have F-scores lower than 0.55 but values of about 0.80 for precision, and confusions only with rougher soil. The classifications

based on mono-frequency radar images are associated with F-scores varying from 0.54 to 0.78. The best performances are obtained using short wavelengths (X- and C-bands) and confusions always concern the wheat and grassland classes, and rapeseed for RS-C HV. In the latter case, the confusion can be explained by the particular geometry of rapeseed, which entails a greater vegetation contribution as soon as the various organs of the plant appear before flowering (Fieuzal et al., 2013).

Classifications based on C-band dual co and cross-polarizations (RS-C-HH-HV; RS-C-VV-VH) give the same results as classifications based purely on bands with the same polarization ($0.78 < \text{F-score} < 0.79$) with confusions less than 10% (RS-C-HH; RS-C-VV). The classification based on all polarizations (RS-C-FP) shows higher precision but degraded F-score, indicating an increase in the false positive rate (Table 3). This combination of polarizations is less suitable than the parallel polarizations. Indeed, the classification performed with the three microwave frequencies avoids all confusions and an increased precision (PAI HH = 0.9), illustrating the complementarity of SAR data for distinguishing smooth bare soil. This increase in precision is not accompanied by a variation in the F-score, due to the increase in the false positive rate and an underestimation of smooth bare soil.

The combination of MS optical and radar images provides contrasting performances, with F-scores ranging from 0.2, for the combination of crossed or vertical polarization with C-band, to 0.94 for FS-2 AP-L ($P > 0.83$). The combinations involving the three radar bands with HH polarization give better performances, whether they are added together (F-score FS-MS All HH = 0.86) or not (F-score = 0.84). The confusions observed with radar mono-frequency disappear with the use of combined optical/radar images but not the confusions with rough soil that affect the optical range. Only the combined use of all wavelengths enables this confusion to be almost completely avoided but the proportion of false positives deteriorates the F-score. This is not the case for the Alos/Formosat-2 combination, for which the F-score reaches 0.94.

Concerning rougher soils, the results are intermediate, with F-scores varying between 0.10 (AP-L) and 0.87 (FS-2 AP-L). For the shortest wavelengths (optical and X-band), the precisions are lower than the F-score, indicating an overestimation of the class. The classifications based only on optical reflectances give F-scores varying between 0.56 and 0.70, with a maximum for the classification using the near infrared. Confusions concern smooth bare soils (explained by the closeness of the reflectance values for the two classes of bare soil: percentage of 8.1 and 7.1 for MR and SR respectively) and to a lesser extent rapeseed

For the classifications using microwaves, the F-score ranges from 0.10 to 0.62 and significant confusions with rapeseed are observed. These can be explained by high levels of backscattering due to the complex geometry of the plant, which induces similar behaviour than a signal backscattered by a rough surface (Fig. 10) (Fieuzal et al., 2013; Betbeder et al., 2016). However, a polarization effect can be noted with particular confusions for the classification performed in VV polarization, with wheat and smooth soils. This is explained by the low levels of backscattering for these surfaces at this period of the year. The plots of wheat are at the stage where the stalks are growing longer (Fig. 4 e), which is expressed by marked attenuation of the signal, particularly in the C-band in VV polarization (Fieuzal et al., 2013; Mattia et al., 2003), while the smooth soil is characterized by specular reflection. For the classifications based on combinations of polarizations (HH/HV, VV/VH or full polar), only confusions with the rapeseed class persist. Finally, the use of three radar frequencies with HH polarization reveals confusions with smooth soil that are absent from mono-frequency classifications.

Optical/radar combinations for the C- and X-bands do not modify the results obtained with the near infrared reflectance alone. Conversely, combining Alos and Formosat-2 enables better results to be obtained, with an F-score of 0.87 (PFS-2-MS-AP-L = 0.97), than the separated use of signals providing F-scores of 0.10 and 0.68. The

complementarity of the signals acquired with the most different wavelengths allows to better discriminate this surface state by taking full advantage of the combined optical and radar domains to avoid confusions.

6. Conclusion and perspectives

This study quantifies the contributions and the complementarities of the different frequencies for detecting 4 types of land use (wheat, barley, rapeseed and grassland) and two states of bare soils (with medium and small roughness), which it appears crucial to identify agricultural practices (i.e., tillage, crop sowing, or cover cropping) through the land use monitoring. The results obtained for these six classes as a whole show that the use of one mono-frequency images provides limited overall results (kappa values below 0.6), as reported in the literature. Nevertheless, certain land use classes are correctly discriminated, with F-scores exceeding 0.8 for wheat and rapeseed.

A significant improvement in the classifications is obtained by fusing images delivered by optical and radar sensors, with kappa values greater than 0.65 for the majority of configurations (70%). These values reach a kappa of 0.81 when Alos/Formosat-2-MS images are paired ($0.64 < OA < 0.85$), a result that proved true for most of the classes studied.

For barley, confusions (with bare soil and to a lesser extent wheat) that affect the classification obtained with Alos and those observed on the classification based on Formosat-2 in multi-spectral images (with vegetated surfaces) largely offset one another, allowing an F-score of 0.56 and a precision of 0.73 to be obtained. For rapeseed, the performance associated to the combined use of optical and radar signals reached 0.98 for 4 different combinations (AP-L-HH/FS-MS, TS-X/FS-MS, All-HH/FS-MS and RS-C-FP/FS-MS). For grassland, from a user's point of view, the best results were again obtained by combining MS images with those acquired in the L-band. On the other hand, the F-score for wheat were slightly less accurate with Alos/Formosat-2 (-0.01), the infrared band being sufficient alone in this period of the phenological cycle.

For smooth bare soil, the combined use of all radar wavelengths was necessary to make a reliable distinction between smooth and rougher soil. However, the percentage of false positives deteriorated the F-score. This was not the case with the Alos/Formosat-2 combination, for which the F-score reached 0.94. For rougher soil, the complementarity of the signals acquired with the most widely separated wavelengths allowed a better discrimination. Thus the advantages of the optical and radar ranges fully avoid confusions and an F-score of 0.87 is obtained.

The complementary nature of the contributions made by signals at very different wavelengths, with the strong penetration of the L-band and the weak penetration of optical waves, was verified not only in the overall result but also for each of the monitored land uses. Images acquired at longer wavelengths thus appear to be very relevant for distinguishing between crops and bare soils, due to the ability of the L-band to provide information on the soil and the geometry of the vegetation.

It seems very interesting to develop the multi-frequency generalization of data at distant wavelengths (L- or even P-bands), by using multi-temporal data, to other land occupations of continental surfaces and for monitoring surface states - possibly even the phases of intercrops. This perspective can be viewed in the context of the Sentinel-2, Alos-2 and TerraSar-L, Biomass missions.

Acknowledgments

The reference data were collected in the framework of the MCM'10 campaign on the Observatoire Spatial Régional (OSR- Regional Space Observatory) zone supported by Observatoire Midi-Pyrénées, Université Paul Sabatier, Toulouse, France, the French national research agency CNRS (Centre National de la Recherche Scientifique), the

French space agency CNES (Centre National d'Etudes Spatiales) and the development research institute IRD (Institut de Recherche pour le Développement). The authors also thank the members of the Kalideos project at CNES and "CS Système d'Informations". Many thanks to the farmers who provided the information needed to know and understand their agricultural land and to all who helped collect data in the field.

References

- Alcantara, C., Kuemmerle, T., Baumann, M., Bragina, E.V., Griffiths, P., Hostert, P., Knorn, J., Müller, D., Prishchepov, A.V., Schierhorn, F., 2013. Mapping the extent of abandoned farmland in Central and Eastern Europe using MODIS time series satellite data. *Environ. Res. Lett.* 8, 035035.
- Amarsaikhan, D., Douglas, T., 2004. Data fusion and multisource image classification. *Int. J. Remote Sens.* 25, 3529–3539.
- Atzberger, C., 2013. Advances in remote sensing of agriculture: context description, existing operational monitoring systems and major information needs. *Remote Sens.* 5, 4124–4124.
- Baillarin, S., Gigord, P., Hagolle, O., 2008. Automatic registration of optical images, a stake for future missions: application to ortho-rectification, time series and mosaic products. *Geoscience and Remote Sensing Symposium*. <https://doi.org/10.1109/IGARSS.2008.4779194>. 2:II-1112-II-1115.
- Bastiaanssen, W.G.M., Molden, D.J., Makin, I.W., 2000. Remote sensing for irrigated agriculture: examples from research and possible applications. *Agric. Water Manag.* 46, 137–155.
- Baghdadi, N., King, C., Bourguignon, A., Remond, A., 2002. Potential of ERS and RADARSAT data for surface roughness monitoring over bare agricultural fields: application to catchments in Northern France. *Int. J. Remote Sens.* 23, 3427–3442.
- Baghdadi, N., Choker, M., Zribi, M., Hajj, M., Paloscia, S., Verhoest, N., Lievens, H., Baup, F., Mattia, F., 2016. A new empirical model for radar scattering from bare soil surfaces. *Remote Sens.* 8, 920.
- Baup, F., Fieuzal, R., Marais Sicre, C., Dejoux, J.-F., le Dantec, V., Mordelet, P., Claverie, M., Demarez, V., Hagolle, O., Lopes, A., Keravec, P., Ceschia, E., Merlin, O., Kidd, R., 2012. MCM'10: An Experiment for Satellite Multispectral Crop Monitoring –From High to Low Resolution Observations, *Geoscience and Remote Sensing Symposium*. 2012. IEEE International, IGARSS. <http://www.cesbio.ups-tlse.fr/us/mcm.html>.
- Baup, F., Villa, L., Fieuzal, R., 2016. Sensitivity of X-band (σ° , γ) and optical (NDVI) satellite data to corn height variation. Accepted in *Advances in Remote Sensing* March 2016.
- Betbeder, J., Rapinel, S., Corgne, S., Pottier, E., Hubert-Moy, L., 2015. TerraSAR-X dual-pol time-series for mapping of wetland vegetation. *Isprs J. Photogramm. Remote Sens.* 107, 90–98.
- Betbeder, J., Fieuzal, N., Baup, F., 2016. Assimilation of LAI and dry biomass derived from optical and microwave satellite images into and agro-meteorological model to estimate soybean yield. Accepted in *J. Select. Top. Appl. Earth Observ. Remote Sens* March 2016.
- Blaes, X., Vanhalle, L., Defourny, P., 2005. Efficiency of crop identification based on optical and SAR image time series. *Remote Sens. Environ.* 96, 352–365.
- Breiman, L., 2001. Random forests. *Mach. Learn.* 45 (1), 5–32.
- Burges, C.J., 1998. *Data Min. Knowl. Discov.* 2, 121.
- Chen, C., Liaw, A., Breiman, L., 2004. Using Random Forest to Learn Imbalanced Data. *Statistics Department*. University of California, Berkeley.
- Chern, J.S., Wu, A.M., Lin, S.F., 2006. Lesson learned from Formosat-2 mission operations. *Acta Astronaut.* 59, 344–350.
- Claverie, M., Demarez, V., Duchemin, B., Hagolle, O., Ducrot, D., Marais Sicre, C., Dejoux, J.F., Huc, M., Keravec, P., Beziat, P., Fieuzal, R., Ceschia, E., Dedieu, G., 2012. Maize and sunflower biomass estimation in southwest France using high spatial and temporal resolution remote sensing data. *Remote Sens. Environ.* 124, 844–857.
- Comaniciu, D., Meer, P., 2002. Mean shift: a robust approach toward feature space analysis. *IEEE Trans. Pattern Anal. Mach. Intell.* 24, 603–619.
- Congalton, R.G., 1991. A review of assessing the accuracy of classifications of remotely sensed data. *Remote Sens. Environ.* 37, 35–46.
- Corgne, S., Dallon, D., Mercier, G., 2014. Land use and land cover monitoring with multitemporal and multipolarization radarsat data: application to an intensive agricultural area (France). *Geoscience and Remote Sensing Symposium (IGARSS), Geoscience and Remote Sensing Symposium, IEEE International, IGARSS 2014*. pp. 4239–4242.
- Cortes, C., Vapnik, V., 1995. Support-vector networks. *Mach. Learn.* 20.
- Du, P., Samat, A., Waske, B., Liu, S., Li, Z., 2015. Random Forest and Rotation Forest for fully polarized SAR image classification using polarimetric and spatial features. *Isprs J. Photogramm. Remote Sens.* 105, 38–53.
- Duchemin, B., Hadria, R., Erraki, S., Boulet, G., Maisongrande, P., Chehbouni, A., Escadafal, R., Ezzahar, J., Hoedjes, J.C.B., Kharrou, M.H., Khabba, S., Mougenot, B., Olioso, A., Rodriguez, J.C., Simonneau, V., 2006. Monitoring wheat phenology and irrigation in Central Morocco: on the use of relationships between evapotranspiration, crops coefficients, leaf area index and remotely-sensed vegetation indices. *Agric. Water Manag.* 79, 1–27.
- Duchemin, B., Fieuzal, R., Augustin Rivera, M., Ezzahar, J., Jarlan, L., Cesar Rodriguez, J., Hagolle, O., Watts, C., 2015. Impact of sowing date on yield and water use efficiency of wheat analyzed through spatial modeling and Formosat-2 images. *Remote Sens.* 7, 5951–5979.
- Duro, D.C., Franklin, S.E., Dubé, M.G., 2012. A comparison of pixel-based and object-based image analysis with selected machine learning algorithms for the classification

- of agricultural landscapes using SPOT-5 HRG imagery. *Remote Sens. Environ.* 118, 259–272.
- Dusseux, P., Corpetti, T., Hubert-Moy, L., Corgne, S., 2014. Combined use of multi-temporal optical and radar satellite images for grassland monitoring. *Remote Sens.* 6, 6163–6182.
- Fieuzal, R., Duchemin, B., Jarlan, L., Zribi, M., Baup, F., Merlin, O., Hagolle, O., Garatuzapayan, J., 2011. Combined use of optical and radar satellite data for the monitoring of irrigation and soil moisture of wheat crops. *Hydrol. Earth Syst. Sci.* 15, 1117–1129.
- Fieuzal, R., Baup, F., Marais Sicre, C., 2012. Sensitivity of TerraSar-x, radarsat-2 and alos satellite radar data to crop variables. *IEEE International Geoscience and Remote Sensing Symposium*. pp. 3740–3743.
- Fieuzal, R., Baup, F., Marais Sicre, C., 2013. Monitoring wheat and rapeseed by using synchronous optical and radar satellite data—from temporal signatures to crop parameters estimation. *Adv. Remote. Sens.* 2013 (2), 162–180.
- Fieuzal, R., Baup, F., 2016. Estimation of leaf area index and crop height of sunflowers using multi-temporal optical and SAR satellite data. *Int. J. Remote Sens.* 37, 2780–2809.
- Fieuzal, R., Marais Sicre, C., Baup, F., 2017. Estimation of sunflower yield using a simplified agrometeorological model controlled by optical and SAR satellite data. *IEEE J. Sel. Top. Appl. Earth Obs. Remote. Sens.*
- Fisette, T., Rollin, P., Aly, Z., Campbell, L., Daneshfar, B., Filyer, P., Smith, A., Davidson, A., Shang, J., Jarvis, I., 2013. AAFC annual crop inventory. *Second International Conference on Agro-Geoinformatics (Agro-Geoinformatics)*. pp. 270–274.
- Fritz, T., Eineder, M., 2008. TerraSAR-X Basic Product Specification Document. TX-GS-DD-3302, Issue 1.9. .
- Gislason, P.O., Benediktsson, J.A., Sveinsson, J.R., 2006. Random Forests for land cover classification. *Pattern Recognit. Lett.* 27, 294–300.
- Hadria, R., Duchemin, B., Baup, F., Le Toan, T., Bouvet, A., Dedieu, G., Le Page, M., 2009. Combined use of optical and radar satellite data for the detection of tillage and irrigation operations: case study in Central Morocco. *Agric. Water Manag.* 96, 1120–1127.
- Hagolle, O., Dedieu, G., Mougnot, B., Debaecker, V., Duchemin, B., Meygret, A., 2008. Correction of aerosol effects on multi-temporal images acquired with constant viewing angles: application to Formosat-2 images. *Remote Sens. Environ.* 112, 1689–1701.
- Hill, M.J., Ticehurst, C.J., Lee, J.S., Grunes, M.R., Donald, G.E., Henry, D., 2005. Integration of optical and radar classifications for mapping pasture type in western Australia. *Ieee Trans. Geosci. Remote. Sens.* 43, 1665–1681.
- Hong, G., Zhang, A., Zho, F., Brisco, B., 2014. Integration of optical and synthetic aperture radar (SAR) images to differentiate grassland and alfalfa in Prairie area. *Int. J. Appl. Earth Obs. Geoinf.* 28, 12–19.
- Hussain, M., Chen, D., Cheng, A., Wei, H., Stanley, D., 2013. Change detection from remotely sensed images: from pixel-based to object-based approaches. *Isprs J. Photogramm. Remote. Sens.* 80, 91–106.
- Jacquemoud, S., Verhoef, W., Baret, F., Bacour, C., Zarco-Tejada, P.J., Asner, G.P., 2009. PROSPECT+SAIL models: a review of use for vegetation characterization. *Remote Sens. Environ.* 113 (1), S56–S66.
- Joshi, N., Baumann, M., Ehammer, A., Fensholt, R., Grogan, K., Hostert, P., Jepsen, M., Kuemmerle, T., Meyfroidt, P., Mitchard, E., Reiche, J., Ryan, C., Waske, B., 2016. A review of the application of optical and radar remote sensing data fusion to land use mapping and monitoring. *Remote Sens.* 8, 70.
- Jung, H.S., Lee, W.J., Zhang, L., 2014. Theoretical accuracy of along-track displacement measurements from multiple-aperture interferometry (MAI). *Sensors* 14, 17703–17724.
- Inglada, J., Vincent, A., Arias, M., Marais Sicre, C., 2016. Improved early crop type identification by joint use of high temporal resolution SAR and optical image time series. *Remote Sens.* 8, 362.
- Lavalle, M., Wright, T., 2009. Absolute Radiometric and Polarimetric Calibration of ALOS PALSAR Products (1). pp. 18.
- Lee, J.-S., 1981. Speckle analysis and smoothing of synthetic aperture radar images. *Comput. Graph. Image Process.* 17, 24–32.
- Lefebvre, A., Sannier, C., Corpetti, T., 2016. Monitoring urban areas with Sentinel-2A data: application to the update of the copernicus high resolution layer imperviousness degree. *Remote Sens.* 8, 606.
- Loosvelt, L., Peters, J., Skriver, H., Lievens, H., Van Coillie, F.M.B., De Baets, B., Verhoest, N.E.C., 2012. Random Forests as a tool for estimating uncertainty at pixel-level in SAR image classification. *Int. J. Appl. Earth Obs. Geoinf.* 19, 173–184.
- Lu, D., Weng, Q., 2007. A survey of image classification methods and techniques for I improving classification performance. *Int. J. Remote Sens.* 28, 823–870.
- MDA, 2000. RADARSAT Data Product Specification (RSI-GS-026). pp. 129.
- Marais Sicre, C., Baup, F., Fieuzal, R., 2014. Determination of the crop row orientations from Formosat-2 multi-temporal and panchromatic images. *ISPRS J. Photogramm. Remote. Sens.* 94, 127–142.
- Marais Sicre, C., Inglada, J., Fieuzal, R., Baup, F., Valero, S., Cros, J., Huc, M., Demarez, V., 2016. Early detection of summer crops using high spatial resolution optical images time series. submitted in. *Remote Sens.*
- Marais Sicre, C., Fieuzal, R., Baup, F., 2017. Apport des images satellites multi-spectrales (optique et radar) pour la classification des surfaces en herbe. *Revue Française de Photogrammétrie et de Télédétection* 215, 25–41.
- McNairn, H., Champagne, C., Shang, J., Holmstrom, D., Reichert, G., 2009a. Integration of optical and Synthetic Aperture Radar (SAR) imagery for delivering operational annual crop inventories. *ISPRS J. Photogramm. Remote. Sens.* 64, 434–449.
- McNairn, H., Shang, J., Jiao, X., Champagne, C., 2009b. The contribution of ALOS PALSAR multi-polarization and polarimetric data to crop classification. *IEEE Trans. Geosci. Remote. Sens.* 47 (12), 5233805. <https://doi.org/10.1109/TGRS.2009.2026052>. pp. 3981–3992.
- McNairn, H., Kross, A., Lapen, D.R., Caves, R., Shang, J., 2014. Early season monitoring of corn and soybeans with TerraSAR-X and RADARSAT-2. *Int. J. Appl. Earth Obs. Geoinf.* 28 (1), 252–259. <https://doi.org/10.1016/j.jag.2013.12.015>.
- Mellor, A., Boukir, S., Haywood, A., Jones, S., 2015. Exploring issues of training data imbalance and mislabeling on random forest performance for large area land cover classification using the ensemble margin. *Isprs J. Photogramm. Remote. Sens.* 105, 155–168.
- Michel, J., Grizonnet, M., 2015. State of the orfeo toolbox. In *Proceedings of the 2015 IEEE International Geoscience and Remote Sensing Symposium (IGARSS) 1336–1339* 26–31 July 2015;.
- Moran, M.S., Alonso, L., Moreno, J.F., Pilar Cendrero Mateo, M., Fernando de la Cruz, D., Montoro, A., 2012. A Radarsat-2 quad-polarized time series for monitoring crop and soil conditions in Barrax, (Spain). *Int. Geosci. Remote Sens. IEEE, Trans* 50, 1057–1070.
- Mountrakis, G., Im, J., Ogole, C., 2011. Support vector machines in remote sensing: a review. *ISPRS J. Photogramm. Remote. Sens.* 66, 247–259.
- Pal, M., 2005. Random forest classifier for remote sensing classification. *Int. J. Remote Sens.* 26, 217–222.
- Pelletier, C., Valero, S., Inglada, J., Champion, N., Marais Sicre, C., Dedieu, G., 2017. Effect of training class label noise on classification performances for land cover mapping with satellite image time series. *Remote Sens.* 9 (2), 173.
- Picard, G., 2002. Modélisation radar des couverts végétaux. Application à la télédétection de couverts forestiers et agricoles, PhD thesis. Centre d'Études Spatiales de la Biosphère, CESBIO.
- Picard, G., Le Toan, T., Mattia, F., 2003. Understanding C-Band Radar backscatter from wheat canopy using a multiple-scattering coherent model. *Int. Geosci. Remote Sens. IEEE* 41, 7.
- Powers, D.M.W., 2011. Evaluation: from precision, recall and F-factor to ROC, informedness, markedness & correlation. *J. Mach. Learn. Technol.* 2, 37–63.
- Qamer, F., Shehzad, K., Abbas, S., Murthy, M.S.R., Xi, C., Gilani, H., Bajracharya, B., 2016. Mapping deforestation and forest degradation patterns in Western Himalaya, Pakistan. *Remote Sens.* 8, 385.
- Seelan, S.K., Laguetta, S., Casady, G.M., Seielstad, G.A., 2003. Remote sensing applications for precision agriculture: a learning community approach. *Remote Sens. Environ.* 88, 157–169.
- Schuster, C., Schmidt, T., Conrad, C., Kleinschmit, B., Foerster, M., 2015. Grassland habitat mapping by intra-annual time series analysis - Comparison of RapidEye and TerraSAR-X satellite data. *Int. J. Appl. Earth Obs. Geoinf.* 34, 25–34.
- Soria-Ruiz, J., Fernandez-Ordóñez, Y., McNairn, H., 2009. Corn monitoring and crop yield using optical and microwave remote sensing. In: Ho, P.-G.P. (Ed.), *Geoscience and Remote Sensing*. InTech, Open Access Publisher Chapter 19.
- Srivastava, P.K., Han, D., Rico-Ramirez, M.A., Bray, M., Islam, T., 2012. Selection of classification techniques for land use/land cover change investigation. *Adv. Space Res.* 50, 1250–1265.
- Steele-Dunne, S.C., McNairn, H., Monsivais-Huertero, A., Judge, J., Liu, P.W., Papanthassiou, K., 2017. Radar remote sensing of agricultural canopies: a review. *Ieee J. Sel. Top. Appl. Earth Obs. Remote. Sens.* 10, 2249–2273.
- Tewkesbury, A.P., Comber, A.J., Tate, N.J., Lamb, A., Fisher, P.F., 2015. A critical synthesis of remotely sensed optical image change detection techniques. *Remote Sens. Environ.* 160, 1–14.
- Ulaby, F.T., Tavakoli, A., Thomas, B.A., 1987. Microwave propagation constant for a vegetation canopy with vertical stalks. *Ieee Trans. Geosci. Remote. Sens.* 25 (6), 714–725.
- Van Rijsbergen, C.J., 1979. *Information Retrieval*. Butterworths, London.
- Vapnik, V., 1979. *Estimation of Dependences Based on Empirical Data*, vol. 27. Nauka, Moscow, pp. 5165–5184 (in Russian) (English translation: Springer Verlag, New York, 1982).
- Waldner, F., Lambert, M.J., Li, W.J., Weiss, M., Demarez, V., Morin, D., Marais Sicre, C., Hagolle, O., Baret, F., Defourny, P., 2015. Land cover and crop type classification along the season based on biophysical variables retrieved from multi-sensor high-resolution time series. *Remote Sens. (Basel)* 7, 10400–10424.